Journal of Wind Engineering & Industrial Aerodynamics 250 (2024) 105767

Contents lists available at ScienceDirect

Journal of Wind Engineering & Industrial Aerodynamics

journal homepage: www.elsevier.com/locate/jweia

A new analytical wind turbine wake model considering the effects of coriolis force and yawed conditions

Reda Snaiki [a,*], Seyedali Makki [b]

[a] Department of Construction Engineering, École de Technologie Supérieure, Université du Québec, Montréal, QC, H3C 1K3, Canada
[b] Department of Mechanical Engineering, École de Technologie Supérieure, Université du Québec, Montréal, QC, H3C 1K3, Canada

ARTICLE INFO

Keywords:
Wind turbine wake
Wake deflection
Analytical model
Coriolis force
Yawed condition

ABSTRACT

Wind turbine wakes significantly affect power production and impose higher loads on downstream turbines. Therefore, the development of accurate and efficient wake models is important for optimizing wind farm layouts and predicting wind turbine performance. This study introduces a novel analytical wake model for yawed wind turbines that incorporates the effects of the Coriolis force. The wake deflection in the far wake region is derived through the application of the principles of mass and momentum conservation. In the near wake, the deflection is assumed to be linear with distance. A Gaussian distribution is assumed for the velocity deficit within the wind turbine wake. Two approaches have been proposed to estimate the onset of the far wake region. While the first approach employs a simplified empirical formula, the second approach utilizes an iteration-based method. The proposed analytical wake model has been validated against computational fluid dynamics (CFD) results. Subsequently, the effects of several important parameters on the wake deflection have been systematically investigated. Overall, the simulation results showed a satisfactory agreement between the CFD results and those obtained from the proposed model. Furthermore, the study concluded that the Coriolis force can exert significant effects on wake deflection, particularly in the far wake region, confirming previous findings from numerical simulations. Due to its simplicity and computational efficiency, the proposed model can be readily used in several applications, including wind farm layout optimization, control and risk assessment.

1. Introduction

In a wind farm, several wind turbines often operate in the downwind wake flow which presents two important challenges: reduced power production due to the flow velocity deficit and increased fatigue damage due to higher turbulence intensity (Vermeer et al., 2003; Barthelmie et al., 2009). As a result, numerous optimization and control strategies have emerged to optimize the performance and lifespan of the wind turbines, including blade pitch and yaw control strategies (Mikkelsen et al., 2013). However, these strategies often require precise predictions of the wake field, taking into account various wind conditions, such as yawed wind turbines. Furthermore, numerous wind farm applications, such as wind farm layout optimization and risk assessment, require a large number of model evaluations to accommodate various conditions, scenarios, and associated uncertainties. Therefore, achieving these goals using high-fidelity numerical models is impractical, and instead, simplified and cost-effective models should be employed.

Various approaches have been proposed to study and analyze the wind flow in wind farms, typically falling into four primary categories: analytical models, computational fluid dynamics, wind tunnel tests, and field experiments. Computational fluid dynamics (CFD) techniques are widely regarded as one of the most pertinent tools for studying the wind field within wind farms (Sanderse et al., 2011; Sheidani et al., 2023; Zhang et al., 2024; Han et al., 2023; Ye et al., 2023). These techniques rely on the Navier-Stokes equations and typically employ two approaches to simulate the wind turbine-induced forces: the generalized actuator disk model (ADM) (Calaf et al., 2010; Wu and Porté-Agel, 2011; Goit and Meyers, 2015) and the actuator line model (ALM) (Witha et al., 2014). Although ALM enables a more detailed simulation of the rotor's aerodynamic behavior compared to ADM, it is considered a costly technique, particularly for large wind farms. In wind farm applications, the Reynolds-averaged Navier-Stokes (RANS) technique has been extensively used to study the wake field within wind farms (Sanderse et al., 2011). While RANS techniques are computationally less expensive than other CFD techniques, their simulation results are often less accurate due to the parametrization of all scales of the turbulence spectrum.

* Corresponding author.
E-mail address: reda.snaiki@etsmtl.ca (R. Snaiki).

https://doi.org/10.1016/j.jweia.2024.105767
Received 1 February 2024; Received in revised form 13 May 2024; Accepted 13 May 2024
Available online 17 May 2024

On the other hand, large-eddy simulation (LES) only parametrizes the smallest scales while resolving the larger ones. LES simulations have demonstrated notable success in simulating the wind field within wind farms (Wu and Porté-Agel, 2011, 2013). However, due to the substantial computational cost associated with these simulations, applying LES techniques to wind farm layout optimization, online control, and risk assessment presents significant challenges (Snaiki and Wu, 2020, 2022).

Wind tunnel experiments have also been utilized to examine the flow structure of wind turbine wakes (Chamorro and Porté-Agel, 2009; Lebron et al., 2012; Aubrun et al., 2013; Hamilton et al., 2015; Murata et al., 2016; Hyvärinen et al., 2018; Uchida and Gagnon, 2022; Huang et al., 2022). The extensive datasets produced by wind tunnel tests have been instrumental in testing and validating the results of various numerical and analytical models. Nevertheless, wind tunnel tests are highly time-consuming and labor-intensive (He et al., 2022, Abdelsalam et al., 2014). Field experiments, on the other hand, overcome the limitations of wind tunnel tests (such as Reynolds number constraints) and offer more realistic measurements of the wind field using various in-situ equipment such as anemometers (Duckworth and Barthelmie, 2008), scanning wind lidars (Machefaux et al., 2015; Bodini et al., 2017; Carbajo Fuertes et al., 2018), and radars (Hirth et al., 2015). The increasingly available field-measurement data can serve as a valuable resource for data-driven techniques (Li et al., 2021; Wu and Snaiki, 2022) and for validating and testing numerical models.

Over the past few decades, substantial efforts have been devoted to advancing analytical wake models (Tian et al., 2015; Sun and Yang, 2018; Cheng et al., 2019; Ge et al., 2019; He et al., 2021; Lopes et al., 2022; Zhang et al., 2023). Their simplicity and computational efficiency have led to their widespread implementation in diverse engineering applications, including wind farm layout optimization, control-oriented strategies, and risk assessment (Gao et al., 2016; Brogna et al., 2020; Jard and Snaiki, 2023, 2024). Most analytical models have been designed to simulate the steady-state velocity deficit in wind turbine wakes (Jensen, 1983; Frandsen et al., 2006; Bastankhah and Porté-Agel, 2014; Keane et al., 2016; Ishihara and Qian, 2018; Schreiber et al., 2020). While they may be less accurate than other models like CFD models, analytical models offer valuable insights into the fundamental physical principles, as they are derived from governing conservation laws. However, the majority of analytical models do not consider the significant effects of the Coriolis force, which has been shown by various studies to have a substantial impact on wake deflection (Van Der Laan and Sørensen, 2017; Nouri et al., 2020). Disregarding the effects of the Coriolis force can consequently affect the wake steering control strategies (Qian et al., 2022). In a recent study by Qian and Ishihara (2022), an analytical wind turbine wake model was introduced that incorporates the effects of the Coriolis force. However, it does not consider yawed conditions, which is crucial for accurately estimating the wake deflection and implementing yaw control strategies in real wind farms.

In this study, a new analytical model is developed to predict the wake deflection by considering several important factors, including the Coriolis force, yaw angle, ambient turbulence intensity, and thrust coefficient. The time-averaged y-momentum and continuity equations are utilized and simplified to derive a mathematical expression for the far wake deflection. In the near wake, the deflection is assumed to be linear with distance. The proposed wake deflection model is coupled with a Gaussian-based wake model, where the normalized velocity deficit in the wake region is estimated using the self-similarity assumption. Two approaches have been proposed for estimating the onset of the far wake region. While the first approach employs a simplified empirical formula, the second one is based on an iteration procedure. The proposed analytical wake model will be validated using CFD results. Following this, the study will systematically investigate the effects of several important parameters on wake deflection.

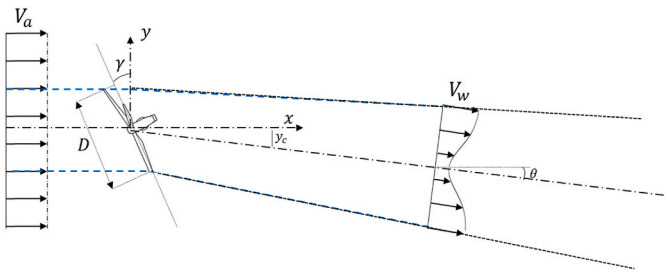

Fig. 1. Schematic representation of the wake deflection.

2. Analytical model

This study introduces a new analytical model to estimate the wake deflection in yawed wind turbines, incorporating the Coriolis force. The model assumes a Gaussian distribution for the velocity deficit and utilizes momentum balance in the lateral direction ('y') and mass conservation equations to derive the wake deflection. Fig. 1 depicts a schematic of wake deflection and boundaries for a yawed wind turbine, where a Gaussian distribution is selected for the spanwise function of the velocity deficit.

The normalized velocity deficit in the wake region is commonly estimated using the self-similarity assumption for both non-yawed and yawed conditions (Bastankhah and Porté-Agel, 2016). Therefore, it can be represented as the product of a streamwise function and a self-similar shape function, as follows:

$$\Delta U / U_a = -F\varphi \tag{1}$$

where $\Delta U = U - U_a$ velocity deficit; U_a = upstream mean wind velocity; U = wake velocity; F = streamwise function for the velocity deficit; and φ = spanwise function for the velocity deficit. The spanwise function φ has frequently been simulated using the Gaussian distribution, expressed as:

$$\varphi = \exp\left(-\frac{r'^2}{2\sigma^2}\right) \tag{2}$$

where $r' = \sqrt{x^2 + (y + y_c)^2}$ distance from the center of the wake in the spanwise direction; y_c = wake deflection; and σ = standard deviation of the mean velocity deficit distribution in the spanwise direction, representing the wake width. On the other hand, the streamwise function in the far wake region can be approximated as (Qian and Ishihara, 2018):

$$F \approx \frac{C_T'}{16\left(\frac{\sigma}{D}\right)^2} = \frac{C_T \cos^3\gamma}{16\left(\frac{\sigma}{D}\right)^2} \tag{3}$$

where C_T = thrust coefficient; γ = yaw angle which is considered positive in the anti-clockwise direction; and D = rotor diameter.

The analytical formula for the wake deflection y_c can be derived from the time-averaged y-momentum equation for the wake, considering the effects of the Coriolis force. This equation can be expressed as (Qian and Ishihara, 2022):

$$u\frac{\partial v}{\partial x} + v\frac{\partial v}{\partial y} + w\frac{\partial v}{\partial z} = -f_c(u - U_g) - \frac{1}{\rho}\frac{\partial p}{\partial y} - \left(\frac{\partial \overline{v'u'}}{\partial x} + \frac{\partial \overline{v'v'}}{\partial y} + \frac{\partial \overline{v'w'}}{\partial z}\right) \tag{4}$$

where ρ = air density; p = pressure; $(u, v, w) = x$, y, and z components of the velocity vector, respectively; $f_c = 2\Omega \sin(\theta)$ Coriolis parameter; Ω =

angular velocity of the Earth's rotation; θ = latitude; U_g = stream-wise component of geostrophic wind; and $(\overline{v'u'}; \overline{v'v'}; \overline{v'w'})$ = Reynold stress tensor. Equation (4) can be simplified since $w \approx 0$ in the wake region, therefore $w\frac{\partial v}{\partial z} \approx 0$. Furthermore, the term $\frac{\partial \overline{v'w'}}{\partial z}$ is two to three orders of magnitude larger than $\frac{\partial \overline{v'u'}}{\partial x}$ and $\frac{\partial \overline{v'v'}}{\partial y}$ (Qian and Ishihara, 2022). Therefore $\frac{\partial \overline{v'u'}}{\partial x}$ and $\frac{\partial \overline{v'v'}}{\partial y}$ can be neglected. Consequently, Eq. (4) can be expressed as:

$$u\frac{\partial v}{\partial x}+v\frac{\partial v}{\partial y}= -f_c(u-U_g)-\frac{1}{\rho}\frac{\partial p}{\partial y}-\left(\frac{\partial \overline{v'w'}}{\partial z}\right) \tag{5}$$

On the other hand, the continuity equation can be expressed as follows:

$$\frac{\partial u}{\partial x}+\frac{\partial v}{\partial y}+\frac{\partial w}{\partial z}=0 \tag{6}$$

This equation can be simplified by considering $\frac{\partial w}{\partial z} \approx c.\frac{\partial v}{\partial y}$, where c is a tuning parameter that can be obtained through state estimation (Boersma et al., 2018). When $c = 0$, Eq. (6) becomes simply $\frac{\partial v}{\partial y} = -\frac{\partial u}{\partial x}$. On the other hand, if $c = 1$, as assumed by Boersma et al. (2018), then $\frac{\partial w}{\partial z} \approx \frac{\partial v}{\partial y}$, implying equal divergence-convergence of streamlines in the y and z directions. The effects of the parameter c on the wake deflection will be investigated in the third section of this paper. Therefore, Eq. (6) becomes:

$$\frac{\partial v}{\partial y}= -\frac{1}{1+c}\frac{\partial u}{\partial x} \tag{7}$$

Substituting Eq. (7) into Eq. (5) results in:

$$u\frac{\partial v}{\partial x}-\frac{v}{1+c}\frac{\partial u}{\partial x}= -f_c(u-U_g)-\frac{1}{\rho}\frac{\partial p}{\partial y}-\left(\frac{\partial \overline{v'w'}}{\partial z}\right) \tag{8}$$

To solve Eq. (8), the decomposition method is used. In this method, each term in Eq. (8) is expressed as the sum of two components: the ambient flow (represented by the symbol a) and the wake-induced component (represented by the symbol Δ). Therefore, Eq. (8) can be rewritten as:

$$(u_a+\Delta u)\frac{\partial(v_a+\Delta v)}{\partial x}-\frac{(v_a+\Delta v)}{1+c}\frac{\partial(u_a+\Delta u)}{\partial x}= -f_c(u_a+\Delta u-U_g) -\frac{1}{\rho}\frac{\partial(p_a+\Delta p)}{\partial y}-\left(\frac{\partial(\overline{v'w'}_a+\Delta\overline{v'w'})}{\partial z}\right) \tag{9}$$

Similarly, the governing equation for the ambient flow can be formulated as:

$$u_a\frac{\partial v_a}{\partial x}-\frac{v_a}{1+c}\frac{\partial u_a}{\partial x}= -f_c(u_a-U_g)-\frac{1}{\rho}\frac{\partial p_a}{\partial y}-\left(\frac{\partial(\overline{v'w'}_a)}{\partial z}\right) \tag{10}$$

Subtracting Eq. (10) from Eq. (9) and assuming that Δp is negligible, along with neglecting the terms $\Delta(.)\frac{\partial(.+\Delta.)}{\partial x}$, results in the following equation:

$$u_a\frac{\partial(\Delta v)}{\partial x}-\frac{v_a}{1+c}\frac{\partial(\Delta u)}{\partial x}= -f_c\Delta u-\left(\frac{\partial(\Delta\overline{v'w'})}{\partial z}\right) \tag{11}$$

The Boussinesq approximation is utilized to represent the Reynolds stress $\Delta\overline{v'w'}$ in the wake region in terms of the added turbulence in the wind turbine wake and wind veer, leading to the following expression:

$$\Delta\overline{v'w'}= -\Delta K\frac{\partial v_a}{\partial z} \tag{12}$$

where ΔK = added turbulent eddy viscosity in the wake region which can be expressed as (Ainslie, 1988):

$$\Delta K= -k_l b_w \Delta u \tag{13}$$

where k_l = empirical parameter equal to $0.015\sqrt{3.56}$ (Ainslie, 1988); and b_w = wake half width which is approximated as $b_w = \sqrt{2\,ln\,2}\sigma$ (Qian and Ishihara, 2018). Dividing Eq. (11) by u_a, then approximating $\frac{\Delta u}{u_a} \approx \frac{-C_T'}{16\left(\frac{\sigma}{D}\right)^2}$ for the far wake, and using the linear expansion of the wake region downstream of the turbine where $\sigma = kx + \varepsilon D$ (Bastankhah and Porté-Agel, 2014) results in the following equation:

$$\frac{\partial\Delta v}{\partial\sigma}=\frac{A}{\sigma^2}+\frac{BC}{\sigma}+\frac{1}{1+c}\frac{v_a}{u_a}\frac{\partial\Delta u}{\partial\sigma} \tag{14}$$

where k = wake growth rate; ε = initial wake width; $A=\frac{f_c C_T' D^2}{16k}$; $B=\frac{0.033 C_T' D^2}{16k}$; and $C=\frac{\partial^2 v_a}{\partial z^2}$. Integrating Eq. (14) from σ_0 (at $x = x_0$ which separates the near and far wake regions) to σ yields the following expression for Δv:

$$\Delta v=\left(-\frac{A}{\sigma}+BCln\sigma-\frac{E}{\sigma^2}\right)-\left(-\frac{A}{\sigma_0}+BCln\sigma_0-\frac{E}{{\sigma_0}^2}\right)+\Delta v_0 \tag{15}$$

where $E=\frac{C_T' D^2 v_a}{16(1+c)}$; and Δv_0 = the value of Δv at $\theta = \theta_0$. On the other hand, the skew angle θ, which indicates the inclination angle of velocity in the wake relative to the upstream velocity, is mathematically defined in terms of the derivative of the wake deflection as follows:

$$\frac{dy_c}{dx}=\theta \approx \frac{v}{u} \approx \frac{v_a+\Delta v}{u_a+\Delta u} \tag{16}$$

It should be noted that the skew angle θ is considered positive in the clockwise direction. Additionally, obtaining an analytical expression of y_c by integrating Eq. (16) using the derived formula of Eq. (15) is extremely challenging. Therefore, the second-order approximation of Taylor expansion of Eq. (16) is first made, which yields the following formula:

$$\frac{dy_c}{dx} \approx \frac{v_a+\Delta v}{u_a}\left(1-\frac{\Delta u}{u_a}+\left(\frac{\Delta u}{u_a}\right)^2\right)=\frac{v_a+\Delta v}{u_a}-\frac{v_a+\Delta v}{u_a}\left(\frac{\Delta u}{u_a}\right) +\frac{v_a+\Delta v}{u_a}\left(\frac{\Delta u}{u_a}\right)^2 \tag{17}$$

By neglecting $\frac{\Delta v}{u_a}\left(\frac{\Delta u}{u_a}\right)^2$, which is small compared to the other terms, Eq. (17) can be simplified to:

$$\frac{dy_c}{d\sigma}=\frac{v_a+\Delta v}{k.u_a}-\frac{v_a}{k.u_a}\left(\frac{\Delta u}{u_a}\right)-\frac{\Delta v}{k.u_a}\left(\frac{\Delta u}{u_a}\right)+\frac{v_a}{k.u_a}\left(\frac{\Delta u}{u_a}\right)^2 \tag{18}$$

Finally, the wake deflection in the far wake can be obtained by integrating Eq. (18) from σ_0 to σ and using the expressions of Δv (i.e., Eq. (15)) along with the approximation $\frac{\Delta u}{u_a} \approx \frac{-C_T'}{16\left(\frac{\sigma}{D}\right)^2}$, resulting in the following expression for y_c:

$$y_c = \frac{M_1}{k.u_a}(\sigma - \sigma_0) + \frac{-A\ln\left(\sigma/\sigma_0\right) + BC(\sigma\, ln\, \sigma - \sigma_0\, ln\, \sigma_0 - \sigma + \sigma_0) + E\left(1/\sigma - 1/\sigma_0\right)}{ku_a} + \frac{H}{u_a}\left[M_1\left(\frac{1}{\sigma_0} - \frac{1}{\sigma}\right) + \frac{A}{2}\left(\frac{1}{\sigma^2} - \frac{1}{\sigma_0^2}\right) + \frac{E}{3}\left(\frac{1}{\sigma_0^3} - \frac{1}{\sigma^3}\right) + BC\left(\frac{1 + ln\,\sigma_0}{\sigma_0} - \frac{1 + ln\,\sigma}{\sigma}\right)\right] + \frac{1}{3}\frac{v_a}{u_a}kH^2\left(\frac{1}{\sigma_0^3} - \frac{1}{\sigma^3}\right) + y_{c0} \tag{19}$$

where $M_1 = \left(\frac{A}{\sigma_0} - BCln\sigma_0 + \frac{E}{\sigma_0^2}\right) + \Delta v_0 + v_a$; and $H = \frac{C_T' D^2}{16k}$. To calculate the wake deflection, the values of x_0, σ_0 and y_{c0} are needed. A simplified approach is employed in this study by assuming the near wake, also known as the potential core, to be linear (Thomas and Ning, 2018), which is represented by the following formula:

$$\frac{y_c(x)}{D} = \theta_0 \frac{x}{D} \tag{20}$$

where θ_0 = initial skew angle which can be expressed as (Coleman et al., 1945):

$$\theta_0 = \frac{0.3\gamma}{\cos\gamma}\left(1 - \sqrt{1 - C_T\cos^3\gamma}\right) \tag{21}$$

The expression of σ_0 can be obtained using the simplified formula proposed by Qian and Ishihara (2018) as:

$$\frac{\sigma_0}{D} = \sqrt{\frac{C_T\, cos^2\,\gamma(sin\,\gamma + 1.88\, cos\,\gamma\theta_0)}{44.4\theta_0}} \tag{22}$$

Other simplified formulas for the length of the potential core are also available (Stanley et al., 2020). However, these simplified estimates are not precise in predicting the near wake length; instead, they provide an initial value for the far wake model (Bastankhah and Porté-Agel, 2016). An approximation for Δv_0 can be provided using the general streamwise function which is applicable to both the near and far wake regions, as proposed by Ishihara and Qian (2018):

$$\Delta v_0 \approx \theta_0 u_a\left[1 - \frac{1}{\left(a + b.\frac{x_0}{D} + p\right)^2}\right] - v_a \tag{23}$$

where (a,b,p) = model parameters derived by Ishihara and Qian (2018) as:

$$\begin{aligned} a &= 0.93C_T^{-0.75}I_a^{0.17}, \\ b &= 0.42C_T^{0.6}I_a^{0.2}, \\ p &= 0.15C_T^{-0.25}I_a^{-0.7}(1 + x_0/D)^{-2} \end{aligned} \tag{24}$$

With the obtained value of x_0, y_{c0} can be calculated as $y_{c0} = \theta_0 x_0$.

To calculate the ambient flow components (u_a, v_a), the Ekman layer assumption is employed here, which considers the flow to be governed by the balance of Coriolis forces, the geostrophic pressure gradient, and surface stress, as detailed below:

$$-f_c v_a = -\frac{1}{\rho}\frac{\partial p_a}{\partial x} + K_0\frac{\partial^2 u_a}{\partial z^2} \tag{25}$$

$$f_c u_a = -\frac{1}{\rho}\frac{\partial p_a}{\partial y} + K_0\frac{\partial^2 v_a}{\partial z^2} \tag{26}$$

where K_0 = turbulent eddy viscosity. The analytical solution of (u_a, v_a) can be then given as (Qian and Ishihara, 2022):

$$u_a = U_g - e^{-az}\left(U_g cosaz + V_g sinaz\right) \tag{27}$$

$$v_a = V_g + e^{-az}\left(-V_g cosaz + U_g sinaz\right) \tag{28}$$

where $= \left(\frac{f_c}{2K_0}\right)^{0.5}$; $U_g = Gcos\Phi_H$; $V_g = -Gsin\Phi_H$; and Φ_H = angular deviation between the wind direction at the hub height of a wind turbine H and the direction of the geostrophic wind.

3. Application

In this section, the proposed model will be validated and analyzed to evaluate the impact of several critical parameters on the response. The wind turbine specifications are based on the offshore 2.4 MW utility-scale wind turbine at the Choshi demonstration site. The rotor diameter D is 92 m and the hub height H is 80 m (Qian and Ishihara, 2022). The ambient inflow wind speed at the hub height is $(u_a, v_a) = (10.20, -0.233)\ m/s$, with the value of v_a approximated based on the work of (Qian and Ishihara, 2022). The turbulent eddy viscosity is $K_0 = 0.24\ m^2/s$ and the Coriolis parameter is taken as $f_c = 1.267 \times 10^{-5}\ rad/s$.

3.1. Model validation

The proposed analytical model is validated using computational fluid dynamics (CFD) results which simulate the turbulent wake flows. These CFD results were obtained from the work of (Qian and Ishihara, 2018). The numerical model is based on the Reynolds Averaged Navier-Stokes (RANS) equations, which were augmented with the Reynolds Stress Model (RSM) to improve the accuracy for complex flows by considering anisotropic turbulence stresses. Notably, the RSM model has demonstrated superior performance compared to standard turbulence models such as the $k - \varepsilon$ model (Cabezon et al., 2011). Additionally, the Linear Pressure-Strain model was utilized to represent the Reynolds stress tensor. The wind turbine is represented by an actuator disk model with rotation to consider the impact of rotor-induced forces on the flow. In this model, lift and drag forces are calculated using the blade element theory (Burton et al., 2011) and then distributed across the actuator disk. The numerical model, based on RSM, has been compared with both large-eddy simulation (LES) and experimental results. These comparisons showed a good agreement between the RSM results, LES results, and the experimental findings (Qian and Ishihara, 2018).

It should be noted that the LES results for the wind turbine wake were validated against high-accuracy experimental data (Qian and Ishihara, 2017). The wind tunnel experiments used spires and fences to simulate different flow types with varying turbulence intensities. For each flow type, experiments were conducted with different wind turbine thrust coefficients. A split-fiber probe was used to measure vertical and horizontal velocity profiles at various locations behind the turbine. To assess the accuracy of the RSM for wind turbine wake simulation, it was compared against both LES results (Qian and Ishihara, 2017) and experimental data (Ishihara et al., 2004). Initially, neutral atmospheric boundary layer profiles without wind turbines were generated and compared. The vertical profiles of mean velocity and turbulence intensity were then compared at several streamwise locations between LES

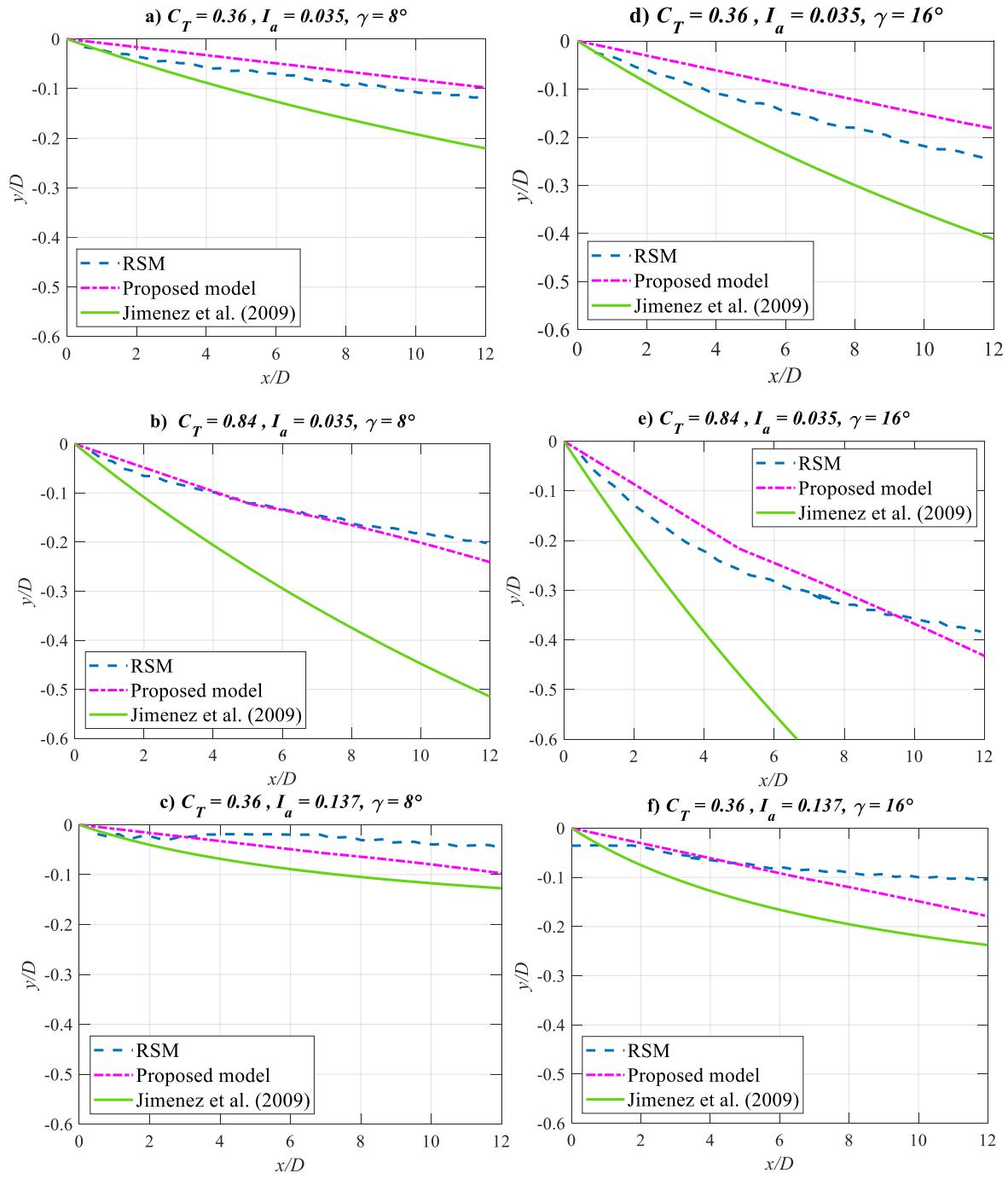

Fig. 2. Validation of the predicted wake deflections under several wind turbine conditions.

Table 1
RMSE of the predicted wake deflections.

	Simulation scenario					
	$C_T = 0.36$ $I_a = 0.035$ $\gamma = 8°$	$C_T = 0.84$ $I_a = 0.035$ $\gamma = 8°$	$C_T = 0.36$ $I_a = 0.137$ $\gamma = 8°$	$C_T = 0.36$ $I_a = 0.035$ $\gamma = 16°$	$C_T = 0.84$ $I_a = 0.035$ $\gamma = 16°$	$C_T = 0.36$ $I_a = 0.137$ $\gamma = 16°$
Proposed model	0.022	0.015	0.031	0.052	0.034	0.042
Jiménez et al. (2009)	0.061	0.187	0.063	0.101	0.329	0.099

results (Qian and Ishihara, 2017), RSM results, and experimental profiles at the turbine location (Ishihara et al., 2004). The comparison involved plotting these profiles together and assessing their agreement. Quantitative comparison using the Normalized Root Mean Square Error (NRMSE) for two cases with ambient turbulence intensities of 0.035 and 0.137 showed that the RSM results agreed well with the LES results and experimental data. The next stage of validation involved examining wake characteristics in the horizontal *x*-*y* plane at hub height. This included normalized mean velocity and turbulence intensity. Two case scenarios were considered: (1) $I_a = 0.137$, $C_T = 0.36$, and (2) $I_a = 0.137$, $C_T = 0.84$. The RSM-predicted horizontal profiles of mean velocity and turbulence intensity at selected downwind locations exhibited good agreement with the experimental data and showed similar

accuracy to the LES results. Additional details are also available in the Appendix.

Fig. 2 illustrates the wake deflections under various conditions, including turbulence intensity, yaw angle, and thrust coefficient. Furthermore, the proposed model has been compared with Jimenez's model (Jiménez et al., 2009). It is important to note that for the simulations presented in Fig. 2, the simplified expression of σ_0 (i.e., Eq. (22)) has been utilized. Additionally, a value of $c = 0$ was chosen, implying that $\frac{\partial w}{\partial z} \approx 0$. Other values of c will also be explored towards the conclusion of this section.

The results of Fig. 2 demonstrate an acceptable agreement between the numerical results and the proposed model. On the other hand, Jimenez's model (Jiménez et al., 2009) tends to overestimate the wake deflection, particularly for higher thrust coefficients (i.e., $C_T = 0.84$). Additionally, Table 1 summarizes the root mean squared error (RMSE) of the predicted results (for both the proposed model and Jimenez's model) compared to the RSM simulation results. It is evident that Jimenez's model yields higher RMSE values for all selected scenarios. Moreover, the accuracy of Jimenez's model decreases with increasing thrust coefficient, as indicated by the higher RMSE values in these cases. It should be noted that Jimenez's model was developed based on momentum conservation principles and the top-hat model proposed by Jensen (1983) for the velocity deficit. However, the assumption of a top-hat shape for the velocity deficit has been shown to be inaccurate (Ishihara et al., 2004; Porté-Agel et al., 2020). These limitations lead to underestimating the velocity deficit at the wake center and overestimating it at the edges. This discrepancy explains the observed deviation in the results. Compared to the top-hat model, a Gaussian distribution offers a more accurate representation of the velocity deficit

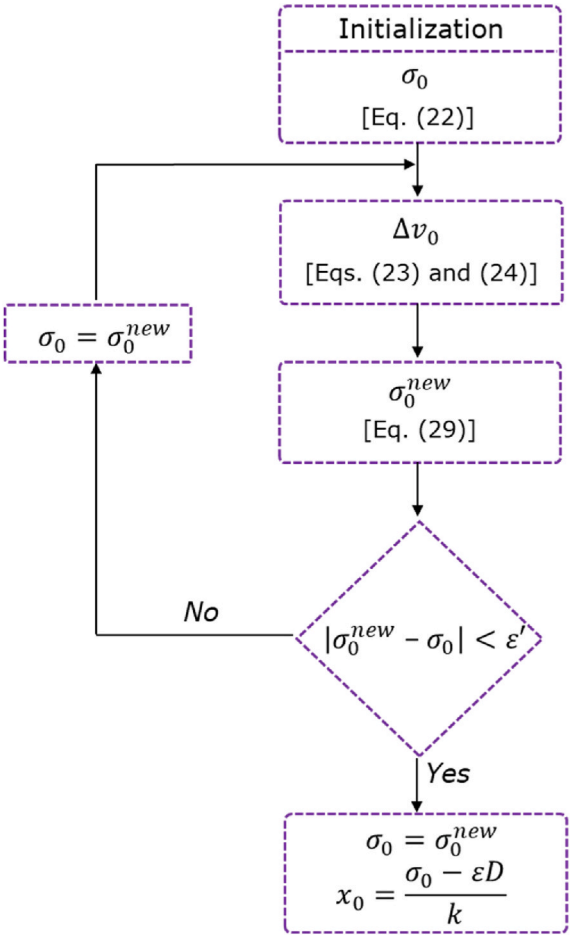

Fig. 3. Flow chart for the determination of σ_0 and x_0.

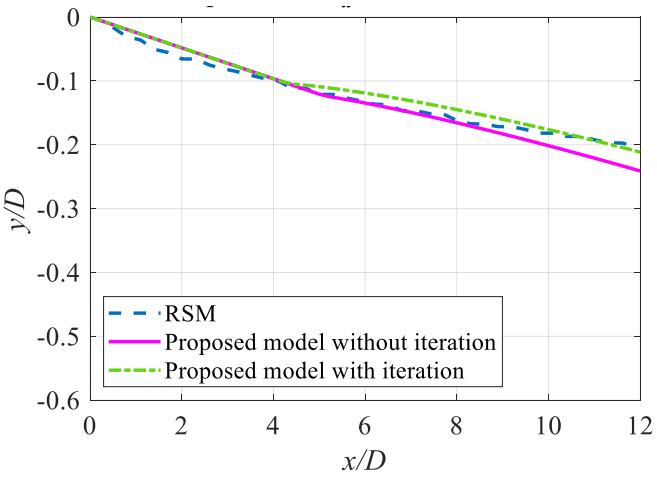

Fig. 4. Comparison between the predicted wake deflection with and without iterations.

profile, as supported by experimental data (Chamorro and Porté-Agel, 2009) and numerical simulations (Xie and Archer, 2015).

It is worth noting that the value of σ_0, and consequently x_0, was determined using the simplified formula from Eq. (22). Other formulas have also been proposed in the literature (Stanley et al., 2020). An alternative method involves considering that the skew angle θ is the same at the joint location (σ_0) of the near and far wake regions (Qian and Ishihara, 2018). Specifically, by equating Eqs. (16) and (21), the expression for σ_0 can be derived as:

$$\frac{\sigma_0}{D} = \sqrt{\left|\frac{C_T' u_a \theta_0}{16(v_a + \Delta v_0 - u_a \theta_0)}\right|} \tag{29}$$

Since σ_0 depends on Δv_0, which is itself dependent on x_0 (and hence σ_0) [Eq. (23)], an iterative approach is necessary to compute the value of σ_0. Fig. 3 outlines the flowchart for calculating σ_0 and its corresponding x_0. Specifically, an initial estimate of σ_0 can be obtained using the approximation in Eq. (22) (Qian and Ishihara, 2018). Once the initial value is known, Δv_0 can be evaluated using Eqs. (23) and (24). The value of σ_0 is then updated to σ_0^{new} until $|\sigma_0^{new} - \sigma_0| < \varepsilon'$, where ε' is a selected threshold. Once σ_0 is determined, the corresponding x_0 can be calculated as $x_0 = \frac{\sigma_0 - \varepsilon D}{k}$.

To analyze the wake deflection using Eq. (29) with the iterative process (Fig. 3), the predicted wake deflection was predicted with (Eq. (29)) and without iteration (Eq. (22)) in Fig. 4. This comparison is based on one simulation scenario with $C_T = 0.84$, $I_a = 0.035$ and $\gamma = 8°$.

As depicted in Fig. 4, the predicted wake deflection with and without iteration closely align for the selected wind turbine scenario. In particular, the predicted values of x_0/D for the simulation without iteration and with iteration are 5.1 and 4.3, respectively. This indicates that the simplified expression of x_0 (Eq. (22)) offers a good approximation of the initial far wake location.

Fig. 5 shows the normalized mean velocity contours and wake deflections in the horizontal $x - y$ plane at the hub height ($z = H$) for a turbine under the same conditions as in Fig. 2. The simulation results suggest that wake deflection increases as the yaw angle increases (Jiménez et al., 2009; Fleming et al., 2014). Moreover, higher thrust coefficients lead to more pronounced wake deflection (Jiménez et al., 2009). Reduced wake deflections and shorter wake regions are also observed with high ambient turbulence intensity due to accelerated flow mixing caused by the high turbulence levels, resulting in faster recovery of both wake deflection and velocity deficit (Bastankhah and Porté-Agel, 2016). Additionally, it is evident that the wake deficit decreases as the yaw angle increases. This is reasonable as larger yaw angles result in a smaller thrust force on the rotor.

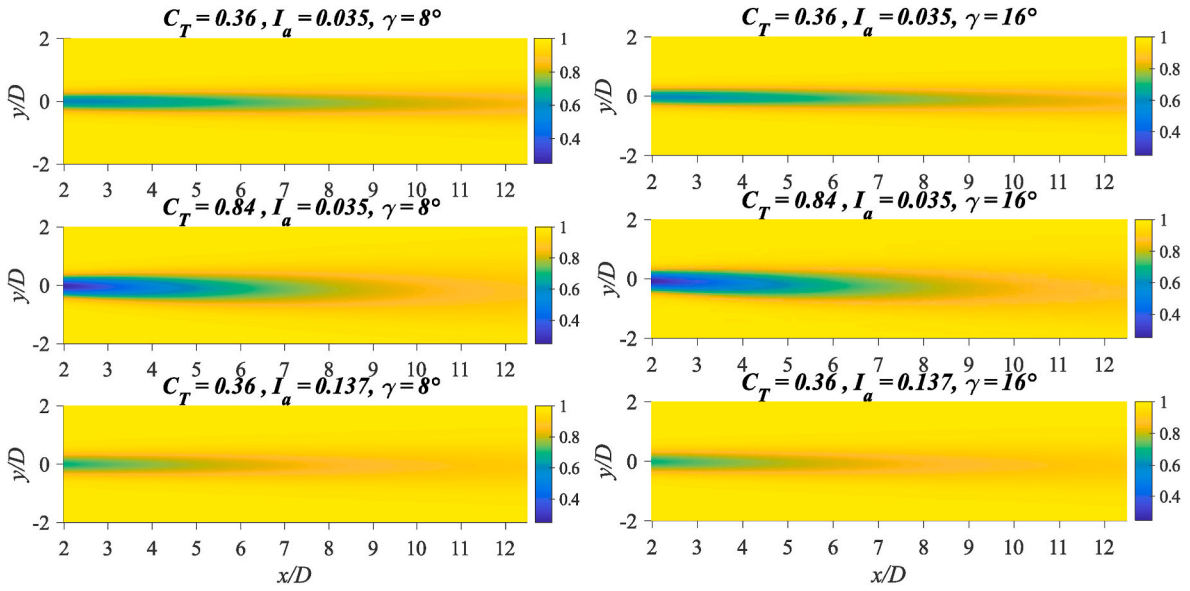

Fig. 5. Normalized horizontal mean wind speed contours at the wind turbine hub height.

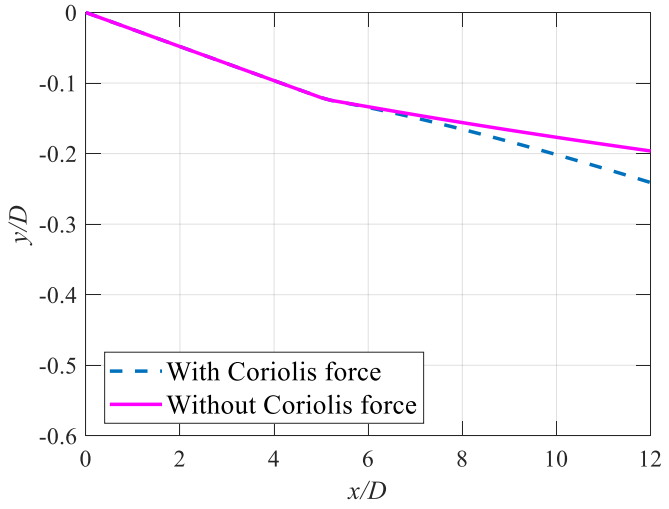

Fig. 6. Predicted wake deflections with and without the consideration of the Coriolis force.

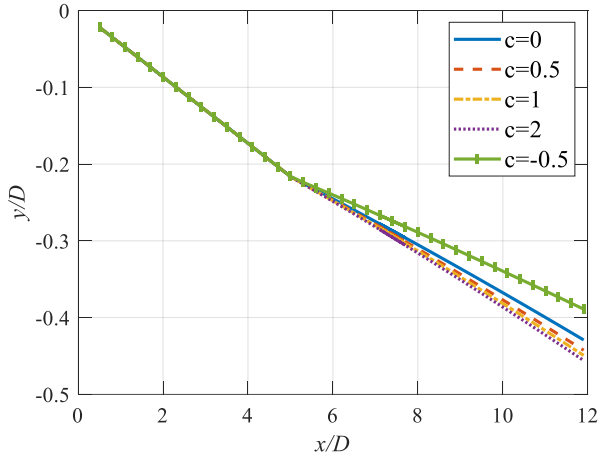

Fig. 7. Comparison of the predicted wake deflection using various c values.

In order to assess the effects of the Coriolis force, one case scenario is selected here, where the wake deflection is plotted both with and without the consideration of the Coriolis force. Fig. 6 depicts the wake deflection for the wind turbine scenario with $C_T = 0.84$, $I_a = 0.035$ and $\gamma = 8°$. It can be concluded that the Coriolis force can have significant effects on the wake deflection, particularly in the far wake. For instance, at $\frac{x}{D} = 12$, the calculated wake deflection ($\frac{y}{D}$) is -0.241 when considering the Coriolis force, compared to -0.196 when not considering it, indicating a 23.5% difference.

The findings of Fig. 6 align with those of previous studies (Van Der Laan and Sørensen, 2017), which demonstrated that the Coriolis force induces a clockwise deflection of wind farm wakes in the northern hemisphere. Consequently, it is important to consider this force, as it can have a substantial impact on wake steering control strategies (Qian et al., 2022).

To investigate the effects of the c values on the wake deflection, a comparison of the predicted wake deflection for various c values is presented in Fig. 7 for the wind turbine scenario with $C_T = 0.84$, $I_a = 0.035$ and $\gamma = 16°$. The simulation results indicate that the value of c can affect the deflection of the far wake, with positive c values resulting in an increase in y_c and negative values leading to a decrease in y_c. Specifically, at $\frac{x}{D} = 12$, the resulting $\frac{y}{D}$ values are -0.429, -0.443 ($+3.26\%$), -0.449 ($+4.66\%$), -0.456 (6.29%) and -0.389 (-9.32%) for c values of 0, 0.5, 1, 2 and -0.5, respectively.

4. Discussion

This work presents a novel analytical wake model for yawed wind turbines incorporating the Coriolis force effects. The model leverages mass and momentum conservation principles to derive wake deflection in the far-wake region. In the near wake, a linear distance dependence is assumed for deflection, while the velocity deficit within the wake follows a Gaussian distribution. Two approaches are proposed for the far-wake onset estimation: a simplified empirical formula and an iteration-based method. The model was validated against CFD results, with a systematic examination of key parameter effects on wake deflection. The simulations demonstrate good agreement between the proposed model and CFD. Additionally, the study emphasizes the significant impact of the Coriolis force on wake deflection, particularly in the far-wake region, supporting prior numerical simulation findings.

While the proposed analytical wake model demonstrates good simulation results for wake deflection, several limitations require

further investigation. Firstly, the derivation of the analytical model involves disregarding some nonlinear terms to facilitate its derivation, a practice supported by several studies. However, a more comprehensive study and sensitivity analysis are necessary to assess the effects of these neglected terms on the overall model performance. Secondly, the assumption of a Gaussian distribution for the velocity deficit (span-wise function) has been made, which outperforms the top-hat profile. Nevertheless, single Gaussian profiles are typically designed to perform well within the far-wake region, where most downstream turbines are located. Therefore, these profiles may not yield satisfactory results for predicting wake velocity within the near-wake region, which often exhibit a double Gaussian profile due to blade lift distribution (Magnusson, 1999; Soesanto et al., 2023). Incorporating a double Gaussian profile into the model could be straightforward and improve near-wake predictions. Thirdly, advanced formulas could be employed to represent the streamwise function for both the near and far wake regions, although this may complicate the derivation of an analytical model. Additionally, a tuning parameter 'c' has been selected within the continuity equation. While past studies suggest simple values (Boersma et al., 2018), implementing online updating schemes via state estimation might be necessary for operational setups to obtain a more accurate 'c'. Furthermore, while the wake deflection was assumed to be linear in the near wake, more realistic representations could be considered for more accurate simulation. However, the primary focus of the present study is the far wake, where most downstream turbines are located. Moreover, while both the simplified empirical formula and iteration-based procedure offer practical solutions for defining wake boundaries, they may not always fully capture the complexities of wake transitions under varying atmospheric conditions and wind turbine configurations. Lastly, the proposed analytical model was validated against high-fidelity numerical results. While this is a common approach, comparing the predicted results with experimental data from wind tunnel tests or field measurements could be beneficial. It should be noted that like most available analytical models, the proposed model is designed for steady-state velocity deficits. Therefore, it cannot capture the transient and unsteady characteristics of the wake field. However, it offers valuable insights into the fundamental physics of yawed wind turbines while considering Coriolis effects. In addition, the model's simplicity and computational efficiency make it a good candidate for real-world applications in wind farm optimization, control strategies, and risk assessments.

5. Conclusion

This study presents a new analytical wake model for yawed wind turbines that accounts for the effects of the Coriolis force. While the wake deflection is derived through the application of mass and momentum conservation principles in the far wake region, a linear assumption is assumed in the near wake region. Then, a Gaussian distribution is used to model the velocity deficit within the wake of the wind turbine. Two approaches have been proposed to estimate the onset of the far wake region. While the first approach relies on a simplified empirical formula, the second approach is based on an iteration-based procedure. In general, the validation of the proposed model against CFD results demonstrates a good overall model's accuracy. This study systematically investigated several key assumptions and parameters. For example, it revealed that considering the Coriolis force in yawed conditions can substantially increase the wake deflection in the far wake for certain scenarios by over 20%. The proposed model offers more flexibility and can be tuned through several parameters (e.g., the c parameter in the continuity equation) that can be obtained through state estimation tailored to specific wind farm applications. The model's simplicity and computational efficiency make it well suited for practical applications in wind farm layout optimization, control strategies, and risk assessment.

CRediT authorship contribution statement

Reda Snaiki: Writing – review & editing, Writing – original draft, Visualization, Validation, Supervision, Software, Resources, Project administration, Methodology, Investigation, Funding acquisition, Formal analysis, Conceptualization. **Seyedali Makki:** Writing – original draft, Visualization, Validation, Software, Methodology, Investigation, Formal analysis.

Declaration of competing interest

The authors declare that they have no known competing financial interests or personal relationships that could have appeared to influence the work reported in this paper.

Data availability

Data will be made available on request.

Acknowledgements

This work was partly supported by the Natural Sciences and Engineering Research Council of Canada (NSERC) [grant number CRSNG RGPIN 2022-03492].

Appendix

This section presents examples of the validation procedures employed to assess the performance of the numerical models used in this study. A more comprehensive validation analysis can be found in Qian and Ishihara (2017) and Qian and Ishihara (2018). One specific validation approach involved a comparison of vertical profiles for the mean velocity at various streamwise locations. This comparison was conducted between the results obtained from LES, RSM simulations, and experimental data collected at the turbine location (Qian and Ishihara, 2018). Fig. 8 provides this comparison by presenting the normalized mean velocity profiles within simulated neutral atmospheric boundary layers (without wind turbines) for two specific values of I_a (0.035 and 0.137).

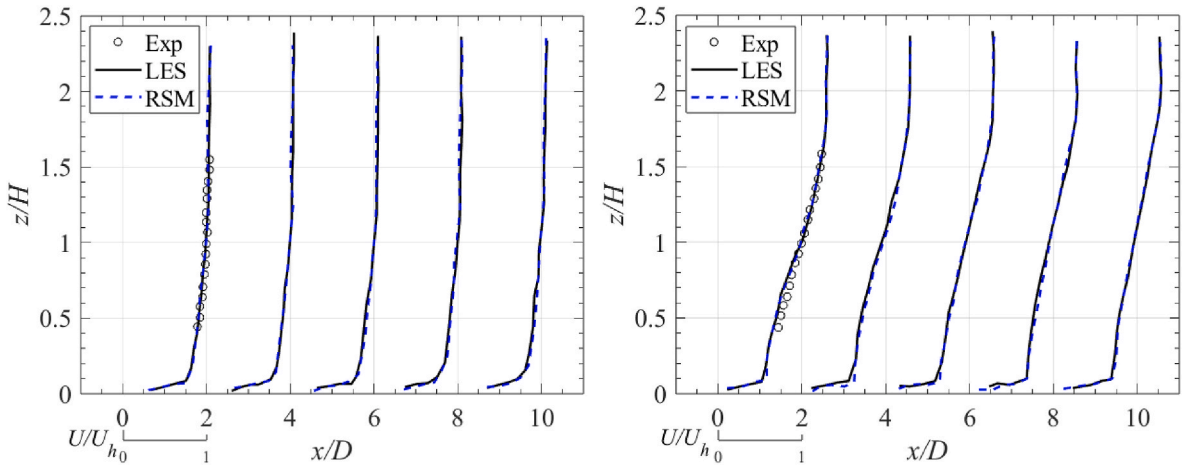

Fig. 8. Vertical profiles of normalized mean velocity in neutral atmospheric boundary layers without wind turbines for $I_a = 0.035$ (left) and $I_a = 0.137$ (right) (Qian and Ishihara, 2018).

The normalized root mean square error (NRMSE) was calculated to quantify the agreement between simulations and experimental data for both normalized mean velocity and turbulence intensity (Qian and Ishihara, 2018). For the normalized mean velocity, both LES and RSM achieved low NRMSE values for $I_a = 0.035$ (0.012 and 0.015, respectively) and $I_a = 0.137$ (0.031 and 0.032, respectively). These results indicate good agreement between the simulated and measured mean velocity profiles. Similarly, for the turbulence intensity, both LES and RSM achieved low NRMSE values for $I_a = 0.035$ (0.24 and 0.26, respectively) and $I_a = 0.137$ (0.10 and 0.13, respectively).

On the other hand, the NRMSE between the simulated and measured normalized mean wind speeds in the horizontal *x-y* plane at hub height under non-yawed conditions were 0.068 and 0.078 for LES and RSM, respectively, in the case of $I_a = 0.137$ and $C_T = 0.36$. Similar NRMSE values (0.078 and 0.075) were observed for LES and RSM when comparing the simulated and measured turbulence intensity (Qian and Ishihara, 2018). For a separate scenario ($I_a = 0.137$ and $C_T = 0.84$), the NRMSE between simulations and measurements for mean wind speed remained comparable (0.071 and 0.074 for LES and RSM, respectively). The NRMSE for turbulence intensity increased slightly to 0.12 and 0.10 for LES and RSM, respectively (Qian and Ishihara, 2018). Fig. 9 provides the comparison of normalized mean velocity across the horizontal plane at hub height. The low NRMSE values for normalized mean wind speed and turbulence intensity indicate that both LES and RSM simulations reasonably matched the experimental data for wake characteristics.

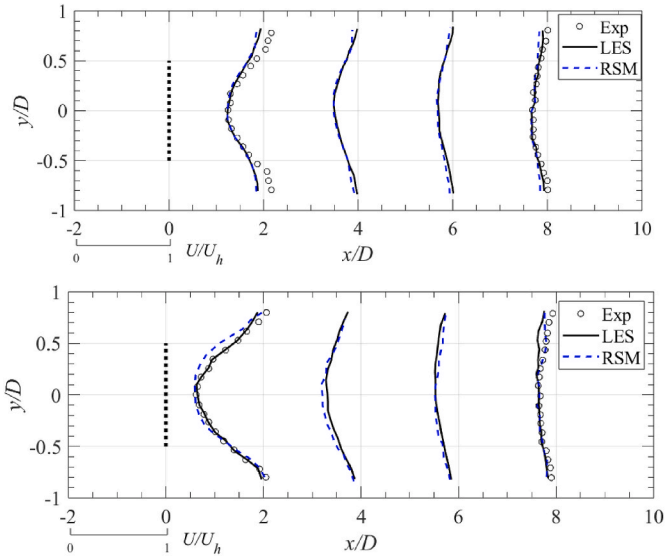

Fig. 9. Normalized mean velocity in the horizontal x-y plane at hub height for $I_a = 0.137$, $C_T = 0.36$ (top) and $I_a = 0.137$, $C_T = 0.84$ (bottom) (Qian and Ishihara, 2018), with the dashed line at $x/D = 0$ indicating the wind turbine location.

References

Abdelsalam, A.M., Boopathi, K., Gomathinayagam, S., Kumar, S.S.H.K., Ramalingam, V., 2014. Experimental and numerical studies on the wake behavior of a horizontal axis wind turbine. J. Wind Eng. Ind. Aerod. 128, 54–65.

Ainslie, J.F., 1988. Calculating the flowfield in the wake of wind turbines. J. Wind Eng. Ind. Aerod. 27 (1–3), 213–224.

Aubrun, S., Loyer, S., Hancock, P.E., Hayden, P., 2013. Wind turbine wake properties: comparison between a non-rotating simplified wind turbine model and a rotating model. J. Wind Eng. Ind. Aerod. 120, 1–8.

Barthelmie, R., Frandsen, S., Hansen, K., Schepers, J., Rados, K., Schlez, W., Neubert, A., Jensen, L., Neckelmann, S., 2009. Modelling the impact of wakes on power output at Nysted and Horns Rev. European Wind Energy Conference, pp. 1351–1373.

Bastankhah, M., Porté-Agel, F., 2014. A new analytical model for wind-turbine wakes. Renew. Energy 70, 116–123.

Bastankhah, M., Porté-Agel, F., 2016. Experimental and theoretical study of wind turbine wakes in yawed conditions. J. Fluid Mech. 806, 506–541.

Bodini, N., Zardi, D., Lundquist, J.K., 2017. Three-dimensional structure of wind turbine wakes as measured by scanning lidar. Atmos. Meas. Tech. 10, 2881–2896.

Boersma, S., Doekemeijer, B., Vali, M., Meyers, J., Van Wingerden, J.-W., 2018. A control-oriented dynamic wind farm model: wfsim. Wind Energy Sci. 3, 75–95.

Brogna, R., Feng, J., Sørensen, J.N., Shen, W.Z., Porté-Agel, F., 2020. A new wake model and comparison of eight algorithms for layout optimization of wind farms in complex terrain. Appl. Energy 259, 114189.
Burton, T., Jenkins, N., Sharpe, D., Bossanyi, E., 2011. Wind Energy Handbook. John Wiley & Sons.
Cabezon, D., Migoya, E., Crespo, A., 2011. Comparison of turbulence models for the computational fluid dynamics simulation of wind turbine wakes in the atmospheric boundary layer. Wind Energy 14, 909–921.
Calaf, M., Meneveau, C., Meyers, J., 2010. Large eddy simulation study of fully developed wind-turbine array boundary layers. Phys. Fluid. 22.
Carbajo Fuertes, F., Markfort, C.D., Porté-Agel, F., 2018. Wind turbine wake characterization with nacelle-mounted wind lidars for analytical wake model validation. Rem. Sens. 10, 668.
Chamorro, L.P., Porté-Agel, F., 2009. A wind-tunnel investigation of wind-turbine wakes: boundary-layer turbulence effects. Boundary-Layer Meteorol. 132, 129–149.
Cheng, Y., Zhang, M., Zhang, Z., Xu, J., 2019. A new analytical model for wind turbine wakes based on Monin-Obukhov similarity theory. Appl. Energy 239, 96–106.
Coleman, R.P., Feingold, A.M., Stempin, C.W., 1945. Evaluation of the induced-velocity field of an idealized helicopter rotor. NACA, Washington, DC, USA, p. 0028.
Duckworth, A., Barthelmie, R.J., 2008. Investigation and validation of wind turbine wake models. Wind Eng. 32, 459–475.
Fleming, P.A., Gebraad, P.M.O., Lee, S., Van Wingerden, J.-W., Johnson, K., Churchfield, M., Michalakes, J., Spalart, P., Moriarty, P., 2014. Evaluating techniques for redirecting turbine wakes using Sowfa. Renew. Energy 70, 211–218.
Frandsen, S., Barthelmie, R., Pryor, S., Rathmann, O., Larsen, S., Højstrup, J., Thøgersen, M., 2006. Analytical modelling of wind speed deficit in large offshore wind farms. Wind Energy: Int. J. Prog. Appl. Wind Power Convers.Technol. 9, 39–53.
Gao, X., Yang, H., Lu, L., 2016. Optimization of wind turbine layout position in a wind farm using a newly-developed two-dimensional wake model. Appl. Energy 174, 192–200.
Ge, M., Wu, Y., Liu, Y., Li, Q., 2019. A two-dimensional model based on the expansion of physical wake boundary for wind-turbine wakes. Appl. Energy 233, 975–984.
Goit, J.P., Meyers, J., 2015. Optimal control of energy extraction in wind-farm boundary layers. J. Fluid Mech. 768, 5–50.
Hamilton, N., Melius, M., Cal, R.B., 2015. Wind turbine boundary layer arrays for Cartesian and staggered configurations-Part I, flow field and power measurements. Wind Energy 18, 277–295.
Han, W., Kim, H., Son, E., Lee, S., 2023. Assessment of yaw-control effects on wind turbine-wake interaction: a coupled unsteady vortex lattice method and curled wake model analysis. J. Wind Eng. Ind. Aerod. 242, 105559.
He, R., Sun, H., Gao, X., Yang, H., 2022. Wind tunnel tests for wind turbines: a state-of-the-art review. Renew. Sustain. Energy Rev. 166, 112675.
He, R., Yang, H., Sun, H., Gao, X., 2021. A novel three-dimensional wake model based on anisotropic Gaussian distribution for wind turbine wakes. Appl. Energy 296, 117059.
Hirth, B.D., Schroeder, J.L., Gunter, W.S., Guynes, J.G., 2015. Coupling Doppler radar-derived wind maps with operational turbine data to document wind farm complex flows. Wind Energy 18, 529–540.
Huang, G., Zhang, S., Yan, B., Yang, Q., Zhou, X., Ishihara, T., 2022. Thrust-matched optimization of blades for the reduced-scale wind tunnel tests of wind turbine wakes. J. Wind Eng. Ind. Aerod. 228, 105113.
Hyvärinen, A., Lacagnina, G., Segalini, A., 2018. A wind-tunnel study of the wake development behind wind turbines over sinusoidal hills. Wind Energy 21, 605–617.
Ishihara, T., Qian, G.-W., 2018. A new Gaussian-based analytical wake model for wind turbines considering ambient turbulence intensities and thrust coefficient effects. J. Wind Eng. Ind. Aerod. 177, 275–292.
Ishihara, T., Yamaguchi, A., Fujino, Y., 2004. Development of a new wake model based on a wind tunnel experiment. Global wind power 105, 33–45.
Jard, T., Snaiki, R., 2023. Real-time repositioning of floating wind turbines using model predictive control for position and power regulation. Wind 3, 131–150.
Jard, T., Snaiki, R., 2024. Real-Time Dynamic Layout Optimization for Floating Offshore Wind Farm Control. *arxiv preprint arxiv:2401.08484*.
Jensen, N.O., 1983. A Note on Wind Turbine Interaction. In: Riso-M-2411, vol. 16. Risoe National Laboratory, Roskilde, Denmark.
Jiménez, Á., Crespo, A., Migoya, E., 2009. Application of a Les technique to characterize the wake deflection of a wind turbine in yaw. Wind Energy 13, 559–572.
Keane, A., Aguirre, P.E.O., Ferchland, H., Clive, P., Gallacher, D., 2016. An Analytical Model for a Full Wind Turbine Wake, 2016. Iop Publishing, 032039.
Lebron, J., Castillo, L., Meneveau, C., 2012. Experimental study of the kinetic energy budget in a wind turbine streamtube. J. Turbul. N43.
Li, S., Snaiki, R., Wu, T., 2021a. Active simulation of transient wind field in a multiple-fan wind tunnel via deep reinforcement learning. J. Eng. Mech. 147, 04021056.
Li, S., Snaiki, R., Wu, T., 2021b. A knowledge-enhanced deep reinforcement learning-based shape optimizer for aerodynamic mitigation of wind-sensitive structures. Comput. Aided Civ. Infrastruct. Eng. 36, 733–746.
Lopes, A.M.G., Vicente, A.H.S.N., Sánchez, O.H., Daus, R., Koch, H., 2022. Operation assessment of analytical wind turbine wake models. J. Wind Eng. Ind. Aerod. 220, 104840.
Machefaux, E., Larsen, G.C., Troldborg, N., Gaunaa, M., Rettenmeier, A., 2015. Empirical modeling of single-wake advection and expansion using full-scale pulsed lidar-based measurements. Wind Energy 18, 2085–2103.
Magnusson, M., 1999. Near-wake behaviour of wind turbines. J. Wind Eng. Ind. Aerod. 80, 147–167.
Mikkelsen, T., Angelou, N., Hansen, K., Sjöholm, M., Harris, M., Slinger, C., Hadley, P., Scullion, R., Ellis, G., Vives, G., 2013. A spinner-integrated wind lidar for enhanced wind turbine control. Wind Energy 16, 625–643.
Murata, J., Endo, M., Maeda, T., Kamada, Y., 2016. Experimental and numerical investigation of the effect of turbulent inflow on a Horizontal Axis Wind Turbine (part II: wake characteristics). Energy 113, 1304–1315.
Nouri, R., Vasel-Be-Hagh, A., Archer, C.L., 2020. The Coriolis force and the direction of rotation of the blades significantly affect the wake of wind turbines. Appl. Energy 277, 115511.
Porté-Agel, F., Bastankhah, M., Shamsoddin, S., 2020. Wind-turbine and wind-farm flows: a review. Boundary-Layer Meteorol. 174, 1–59.
Qian, G.-W., Ishihara, T., 2018. A new analytical wake model for yawed wind turbines. Energies 11, 665.
Qian, G.-W., Song, Y.-P., Ishihara, T., 2022. A control-oriented large eddy simulation of wind turbine wake considering effects of Coriolis force and time-varying wind conditions. Energy 239, 121876.
Qian, G.W., Ishihara, T., 2017. A numerical study of wind turbine wake by large eddy simulation and proposal for a new analytical wake model. Proceedings of the Offshore Wind Energy, London, Uk, pp. 6–8.
Qian, G.W., Ishihara, T., 2022. A NEW WIND TURBINE WAKE MODEL CONSIDERING THE EFFECT OF CORIOLIS FORCE, vol. 25. Japan Council for Renewable Energy, 2022 2022.
Sanderse, B., Van Der Pijl, S.P., Koren, B., 2011. Review of computational fluid dynamics for wind turbine wake aerodynamics. Wind Energy 14, 799–819.
Schreiber, J., Balbaa, A., Bottasso, C.L., 2020. Brief communication: a double-Gaussian wake model. Wind Energy Sci. 5, 237–244.
Sheidani, A., Salavatidezfouli, S., Stabile, G., Rozza, G., 2023. Assessment of URANS and LES methods in predicting wake shed behind a vertical axis wind turbine. J. Wind Eng. Ind. Aerod. 232, 105285.
Snaiki, R., Wu, T., 2020. Revisiting hurricane track model for wind risk assessment. Struct. Saf. 87, 102003.
Snaiki, R., Wu, T., 2022. Knowledge-enhanced deep learning for simulation of extratropical cyclone wind risk. Atmosphere 13, 757.
Soesanto, Q.M.B., Yoshinaga, T., Iida, A., 2023. A linear wake expansion function for the double-Gaussian analytical wake model. Energy Sci. Eng. 11, 1925–1944.
Stanley, A.P.J., King, J., Bay, C., Ning, A., 2020. A Model to Calculate Fatigue Damage Caused by Partial Waking during Wind Farm Optimization, vol. 2020. Wind Energy Science Discussions, pp. 1–34.
Sun, H., Yang, H., 2018. Study on an innovative three-dimensional wind turbine wake model. Appl. Energy 226, 483–493.
Thomas, J.J., Ning, A., 2018. A Method for Reducing Multi-Modality in the Wind Farm Layout Optimization Problem, 2018. IOP Publishing, 042012.
Tian, L., Zhu, W., Shen, W., Zhao, N., Shen, Z., 2015. Development and validation of a new two-dimensional wake model for wind turbine wakes. J. Wind Eng. Ind. Aerod. 137, 90–99.
Uchida, T., Gagnon, Y., 2022. Effects of continuously changing inlet wind direction on near-to-far wake characteristics behind wind turbines over flat terrain. J. Wind Eng. Ind. Aerod. 220, 104869.
Van Der Laan, M.P., Sørensen, N.N., 2017. Why the Coriolis force turns a wind farm wake clockwise in the Northern Hemisphere. Wind Energy Sci. 2, 285–294.
Vermeer, L.J., Sørensen, J.N., Crespo, A., 2003. Wind turbine wake aerodynamics. Prog. Aero. Sci. 39, 467–510.
Witha, B., Steinfeld, G., Heinemann, D., 2014. Advanced Turbine Parameterizations in Offshore LES Wake Simulations, 2014, pp. 8–13.
Wu, T., Snaiki, R., 2022. Applications of machine learning to wind engineering. Front. Built. Environ. 8, 811460.
Wu, Y.-T., Porté-Agel, F., 2011. Large-eddy simulation of wind-turbine wakes: evaluation of turbine parametrisations. Boundary-Layer Meteorol. 138, 345–366.
Wu, Y.-T., Porté-Agel, F., 2013. Simulation of turbulent flow inside and above wind farms: model validation and layout effects. Boundary-Layer Meteorol. 146, 181–205.
Xie, S., Archer, C., 2015. Self-similarity and turbulence characteristics of wind turbine wakes via large-eddy simulation. Wind Energy 18, 1815–1838.
Ye, M., Chen, H.-C., Koop, A., 2023. Verification and validation of CFD simulations of the NTNU BT1 wind turbine. J. Wind Eng. Ind. Aerod. 234, 105336.
Zhang, D., Liu, Z., Li, W., Cheng, L., Hu, G., 2024. Numerical investigation of wind turbine wake characteristics using a coupled Cfd-Csd method considering blade and tower flexibility. J. Wind Eng. Ind. Aerod. 244, 105625.
Zhang, S., Gao, X., Lin, J., Xu, S., Zhu, X., Sun, H., Yang, H., Wang, Y., Lu, H., 2023. Discussion on the spatial-temporal inhomogeneity characteristic of horizontal-axis wind turbine's wake and improvement of four typical wake models. J. Wind Eng. Ind. Aerod. 236, 105368.